Supplementary Information

Contents

1 Asteroseismic Model

In order to extract signatures of stellar rotation from the asteroseismic p mode frequencies, we built a model that simultaneously treats the convective background ($B(\nu)$), the oscillations ($O(\nu)$), and the white noise (W), where ν is frequency [1]. Our data, observed with *Kepler*, are also subject to the apodization (attenuation) of signals in the frequency-domain, where we fit our model [2]. The apodization in power is given by

$$\eta^2(\nu) = \mathrm{sinc}^2\left(\frac{\pi}{2}\frac{\nu}{\nu_{\mathrm{nyq}}}\right), \tag{1}$$

where ν_{nyq} is the Nyquist frequency for the *Kepler* short cadence, which was treated as a free parameter in our model to account for gaps in the data. Apodization only affects signals with characteristic timescales, meaning that it does not affect the white noise level, only the oscillations and convective background components. Given the above, our comprehensive model for the power spectrum is

$$M(\nu) = W + \eta^2(\nu)[O(\nu) + B(\nu)]. \tag{2}$$

1.1 Convective Background ($B(\nu)$)

To model the convective background we used three Harvey components [3], which express the background in power as Lorentzian-like functions centered on zero frequency. The Harvey components take the form

$$H(\nu, a, b, x) = \frac{4a^2/b}{1 + (2\pi b\nu)^x}, \tag{3}$$

where a and b are the free parameters in our model, and x is fixed. The three Harvey components together form our background function as

$$B(\nu) = H(\nu, a, b, x = 4) + H(\nu, c, d, x = 4) + H(\nu, j, k, x = 2), \tag{4}$$

where we have labeled parameters for the separate components. The $x = 2$ term here contributes to the background at high frequencies, whereas the $x = 4$ terms contribute the background at low frequencies.

1.2 Modes of Oscillation ($O(\nu)$)

Modes of oscillation appear in the power spectrum as Lorentzian peaks [4]. These peaks can be described by three values: the radial order (n, the overtone number of the oscillation), the angular degree (ℓ) and the azimuthal order (m). Due to stellar rotation, each mode with an angular degree of $\ell > 0$ is split into its ($2\ell + 1$) Lorentzian components, labeled by m. For all $\ell = (0, 1, 2)$ modes identified for our targets in the 'Kages' and LEGACY studies [5, 6] we add a (set of) Lorentzian(s) to our model, building a composite model representing all visible modes. The construction of our oscillation model takes the form

$$O(\nu) = \sum_n \sum_\ell \sum_{m=-\ell}^{\ell} \frac{H_{n,\ell,m}}{1 + \frac{4}{\Gamma_{n,\ell}^2}(\nu - \nu_{n,\ell,m})^2}, \tag{5}$$

where $H_{n,\ell,m}$ is the height of the mode, $\Gamma_{n,\ell}$ is the linewidth of the mode (approximated to be equal for all split azimuthal orders at a single n and ℓ) and $\nu_{n,\ell,m}$ is the frequency of the mode. The range of n differs per star depending on how many radial orders were reported in LEGACY or Kages, and the range of ℓ depends on how many angular degrees were reported for the corresponding radial order.

1.2.1 Mode Frequencies and Rotational Splitting ($\nu_{n,\ell,m}$)

The mode frequencies of main sequence stars are described by the asymptotic expression [7, 8]. The asymptotic expression defines the locations of the modes as regularly spaced, with structured deviation around $\nu_{\max}$, the frequency of maximum oscillation amplitude. The expression takes the form

$$\nu_{n,\ell,m} = \Delta\nu \left(n + \epsilon + \delta\nu_{0\ell} + \frac{\alpha}{2}(n - \frac{\nu_{\max}}{\Delta\nu} + \epsilon)^2 \right) + m\nu_s \,, \tag{6}$$

where $\Delta\nu$ is the large frequency separation between two consecutive radial orders n, ϵ is a a phase offset, $\delta\nu_{0\ell}$ is the small frequency separation between two oscillation modes of different ℓ at the same radial order, α describes the curvature of the spacing around $\nu_{\max}$, and ν_s is the rotational splitting. Note that here we have expressed the small separation $\delta\nu_{0\ell}$ as a fraction of $\Delta\nu$. In order to improve the computational efficiency of this analysis, we fixed $\Delta\nu$ to the values reported in LEGACY and Kages.

Instead of calculating mode frequencies directly from Equation 6 for the model, we treated the individual mode frequencies as parameters as well, drawn from Equation 6. This is called a 'latent parameter' implementation [9, 10], as it forms a step between the parameters we want to draw inference on (also called hyperparameters) and our data. The parameters $\nu_{n,\ell,m}$ were allowed to vary within an uncertainty σ_ℓ, which has a single value for each angular degree and also varied as a free parameter. This allowed us to account for small shifts in frequency due to sudden changes in the stellar structure [11].

The mode frequency latent parameters were drawn from a normal distribution using Equation 6 as its mean function, as

$$\nu_{n,\ell,m} \sim \mathcal{N}(\nu_{n,\ell,m}, \sigma_\ell) \,, \tag{7}$$

where the expression $\nu_{n,\ell,m}$ on the right hand side represents the contents of Equation 6, and $\mathcal{N}$ represents a normal distribution with a mean equal to $\nu_{n,\ell,m}$ and a standard deviation equal to σ_ℓ. The symbol '$\sim$' indicates that the parameters on the left hand side of the equation are drawn from the probability distribution on the right hand side. This notation will be used throughout this work.

1.2.2 Mode Linewidth ($\Gamma_{n,\ell}$)

The linewidths of asteroseismic p modes vary roughly as a function of mode frequency, and do so slowly relative to $\Delta\nu$. This can be expressed as an empirical relation [6, 12, 13]. However, this relation has six free parameters, none of which are directly relevant to this work. Instead of fitting this relation, we chose to employ a more flexible Gaussian Process [14, GP] to act as a prior on the linewidths. This can be considered as us modelling the linewidths as correlated measurements, effectively loosely constraining how linewidth varies with frequency.

A GP is defined by a covariance kernel (describing the degree of correlation between linewidths) and a mean function (describing a global trend with frequency). As this approach describes the mode linewidths relative to one another in frequency, the radial orders of each target n were rescaled to be between 0 (for the lowest n) and 1 (for the highest n). The radial orders of $\ell = 2$ modes were increased by 1 to ensure this approximation applied to all modes. This approximation was used to describe the change in linewidth as a function of frequency without depending on the exact frequencies of the modes, which themselves were free parameters (see above). Given this, we defined our GP covariance kernel as a Squared Exponential Kernel to capture the slight periodicity of linewidth with frequency, as

$$K_{i,j} = \rho^2 \exp\left[-\frac{(n_{\mathrm{f},i} - n_{\mathrm{f},j})^2}{2L^2} \right] \,, \tag{8}$$

where n_{f} is the fractional radial order of a given mode and $K_{i,j}$ represents an element of the covariance matrix $\underline{K}$, describing the covariance between two values of linewidth at different fractional radial orders. The GP kernel has two hyperparameters: ρ, which determines the spread of the kernel in linewidth, and L, which determines the length scale in terms of n_{f}. The length scale L was significantly larger than the large frequency separation ($\Delta\nu$) in all cases, and so we considered the use of fractional radial orders a valid approximation in this model.

A linear function was used for the mean of the GP, as

$$\mu = m \times n_{\mathrm{f}} + c \,, \tag{9}$$

where m and c are the slope and intercept of the line. The linewidth latent parameters were then drawn from the multivariate probability distribution

$$\Gamma \sim \mathcal{N}(\mu, \underline{K}) \,, \tag{10}$$

where Γ represents the linewidths of all the modes in the model. The parameters m, c and ρ were marginalised over, whereas L was fixed to a pre-determined value.

1.2.3 Mode Heights and Angle of Inclination ($H_{n,\ell,m}$)

The height in power of each mode, $H_{n,\ell,m}$, varies not only as a function of distance in frequency from ν_{max}, but also due to observation conditions, such as inclination angle and passband. In our model, we treated $H_{n,\ell,m}$ as a deterministic parameter, as

$$H_{n,\ell,m} = \varepsilon_{\ell,m}(i)\frac{2(A_{n,\ell})^2}{\pi\Gamma_{n,\ell}} \,, \tag{11}$$

where $\varepsilon_{\ell,m}(i)$ modulates the height as a function of inclination angle i (see below), and $A_{n,\ell}$ and $\Gamma_{n,\ell}$ are the mode amplitude and linewidth respectively for a given radial order and angular degree. Instead of modeling and modulating height directly, we instead sampled in amplitude and linewidth. This approach mitigates the correlations between height and linewidth in the sampling process [15].

As done above for the mode frequencies and linewidths, the mode amplitudes $A_{n,\ell}$ were also treated as latent parameters drawn from a probability distribution governed by hyperparameters. For this, we used a Gaussian function $G(\nu)$, centered on ν_{max}, as

$$G(\nu) = A \times \exp\left[-\frac{(\nu - \nu_{\mathrm{max}})^2}{2w^2}\right] \,, \tag{12}$$

where A is the modes' amplitude at ν_{max}, and w is the width of the Gaussian, both free parameters in our model. The mode amplitude latent parameters were then drawn from the probability distribution

$$A_{n,\ell} \sim \mathcal{N}(G(\nu_{n,\ell}) \times V_\ell, \sigma_A) \,, \tag{13}$$

where V_ℓ is a free parameter for the mode visibility of different angular degrees, which should be consistent for all *Kepler* observations. These parameters describe the difference in relative height between modes of different radial order. The mode visibility for V_0 is fixed at 1, and

$V_{1,2}$ are treated as free parameters. The parameter σ_A, the uncertainty on the distribution, is also a free parameter, and takes the same value for all amplitudes regardless of angular degree.

The angle of inclination of a star with respect to Earth changes the net perturbation by a given mode when integrated across the stellar disc, changing the amplitudes of modes of different azimuthal orders. This is a geometric problem, and is expressed by $\varepsilon_{\ell,m}(i)$, which takes the form [16]

$$\varepsilon_{\ell,m}(i) = \frac{(\ell - |m|)!}{(\ell + |m|)!} \left[P_\ell^{|m|}(\cos(i)) \right]^2 ,\tag{14}$$

where $P_\ell^{|m|}$ are associated Legendre functions. For the first three angular degrees, Equation 14 takes the form [17]

$$\begin{aligned}
\varepsilon_{0,0}(i) &= 1 , \\
\varepsilon_{1,0}(i) &= \cos^2(i) , \\
\varepsilon_{1,\pm 1}(i) &= \frac{1}{2} \sin^2(i) , \\
\varepsilon_{2,0}(i) &= \frac{1}{4}(3\cos^2(i) - 1)^2 , \\
\varepsilon_{2,\pm 1}(i) &= \frac{3}{8} \sin^2(2i) , \\
\varepsilon_{2,\pm 2}(i) &= \frac{3}{8} \sin^4(i) ,
\end{aligned}\tag{15}$$

where the sum of available components for a single ℓ are normalized to one.

1.3 Likelihood Function for $M(\nu)$

If data have Gaussian noise in the time domain, they will appear in the frequency domain with noise following a χ^2 distribution with two degrees of freedom [18, χ_2^2 hereafter]. The noise properties of χ_2^2 distributed data are multiplicative, and require a specific treatment when fitting a model. As our frequency bins can be approximated to be independent, we used the likelihood function [19],

$$\ln p(\mathcal{P}|M(\nu)) = \sum_{j=0}^{N-1} \left[\ln[M_j(\nu)] + \frac{\mathcal{P}_j}{M_j(\nu)} \right] ,\tag{16}$$

where $\mathcal{P}$ is the power spectral density (and thus our data), and $M(\nu)$ represents our model. The subscript j denotes an individual datum, for a total of N data. We have omitted the dependence of the model $M(\nu)$ on its parameters, for clarity. This equation is functionally equivalent to the evaluation of a gamma distribution of the form $\gamma(\mathcal{P}|1, \beta)$, where $\beta = 1/M(\nu)$, which is the implementation we used in the sampling process.

1.4 Model preparation and hyperparameter priors

1.4.1 Fitting the convective background

Fitting the convective background, apodization and white noise component must be done for the full range of the power spectrum in order to be accurately constrained. However, fitting a single model to the full range of frequencies is computationally inefficient when we are interested in the modes of oscillation, as these occupy a relatively small range of frequencies.

In order to speed up this process, the background was first fit independently to a subset of our data for each star. This subset was created by removing all frequencies within a range $0.1 \times \Delta\nu$ below and above the minimum and maximum mode frequencies reported in LEGACY and Kages. For KIC 3427720 we also removed frequencies in the range $90\,\mu\text{Hz} < \nu < 400\,\mu\text{Hz}$, where there were large peaks not of asteroseismic origin, skewing the background fit.

For each star the model function (see Eq. 2) was fit, as

$$M_B(\nu) = W + \eta^2(\nu)B(\nu)\,, \tag{17}$$

where $B(\nu)$ is the background model described in Equation 4. The parameter components of our background fit are then $\phi_B = \{\log(a), \log(b), \log(c), \log(d), \log(j), \log(k), W, \nu_{\text{nyq}}\}$, where the parameters of the Harvey components were sampled in log space. The model was fit to the background data using `PyStan` [20], run for 10,000 iterations on each star.

1.4.2 Obtaining First Guesses and Prior Values

In order to utilise some of the prior measurements of our targets without using them as hard constraints on our parameters, some of our model equations were fit to LEGACY and 'Kages' data to obtain first guesses and mean values on hyperparameter priors.

For first guesses for parameters in the asymptotic expression, we fit Equation 6, *not* including the rotational component $m\nu_s$, to the $\ell = (0, 1, 2)$ mode frequencies reported in LEGACY and 'Kages' for each star, using their reported uncertainties. This yielded estimates of $\hat{\epsilon}$, $\widehat{\delta\nu_{01}}$, $\widehat{\delta\nu_{02}}$ and $\hat{\alpha}$, where the hat symbol '$\,\hat{}\,$' indicates a prior value (e.g. $\hat{\nu}_{\text{max}}$ is taken from LEGACY or 'Kages'). While not precise, as we did not mitigate any perturbations due to acoustic glitches, these rough results act as functional first guesses and prior mean values. The relation was fit to each star using PyMC3 [21] using 5000 iterations on 4 chains.

To obtain first guesses for the parameters used to set the GP prior on linewidth, we fit a GP constructed as in Equation 10 to the linewidths of the $\ell = 0$ modes reported in LEGACY. Linewidths were not reported for the other angular degrees in LEGACY, but the estimates may be generalised to other ℓ, as linewidth is a strong function of frequency. The relation was fit to each star using PyMC3 using 2500 iterations on 4 chains.

Fitting the LEGACY linewidths yielded rough estimates of $\hat{m}$, $\hat{c}$, $\hat{\rho}$ and L for each star. As is noted in Equation 10, L was fixed to this fit value when fitting our full model to our data. For stars in 'Kages', for which no linewidths were reported, we instead fixed these prior values to $\hat{m} = 1$, $\hat{c} = 0.5$, $\hat{\rho} = 0.1$, and the length scale to $L = 0.3$. These values were chosen to reflect those found for the LEGACY stars.

Finally, we obtained prior values for the Gaussian function describing the distribution of mode amplitudes around ν_{max} (Eq. 12). The mode amplitude of the highest peak in the

spectrum was used for $\hat{A}$, which was typically at or near $\nu_{\max}$. For the width of the Gaussian we used the empirical function [6]

$$\hat{w} = 0.25 \times \hat{\nu}_{\max}, \ . \tag{18}$$

For the mode visibilities, we used $\hat{V}_1 = 1.2$ and $\hat{V}_2 = 0.7$, which reflect the results for these parameters reported in the LEGACY catalogue.

1.4.3   Priors on our Hyperparameters

Given our first guesses and measured prior values, we can define the prior probabilities of the hyperparameters on which our model depends. For the mode frequency hyperparameters (Eq. 6), these are

$$
\begin{aligned}
\nu_{\max} &\sim \mathcal{N}(\hat{\nu}_{\max}, 10)\,, \\
\epsilon &\sim \mathcal{N}(\hat{\epsilon}, 1)\,, \\
\alpha &\sim \ln\mathcal{N}(\ln(\hat{\alpha}), 0.01)\,, \\
\delta\nu_{01} &\sim \ln\mathcal{N}(\ln(\widehat{\delta\nu}_{01}), 0.1)\,, \\
\delta\nu_{02} &\sim \ln\mathcal{N}(\ln(\widehat{\delta\nu}_{02}), 0.1)\,, \\
\sigma_{0,1,2} &\sim \mathcal{C}_{1/2}(\beta = 2)\,,
\end{aligned}
\tag{19}
$$

where $\ln\mathcal{N}$ represents a log-Normal distribution and $\mathcal{C}_{1/2}$ represents a half-Cauchy distribution. The half-Cauchy distribution ensures the standard deviations do not inflate to large numbers, and is generally well-behaved close to zero in the case of stars with little deviation from Eq. 6 [22]. Other symbols are as described above. All three hyperparameters $\sigma_{0,1,2}$ describing the uncertainty on the latent parameters of different angular degree were subject to the same prior.

For the mode linewidths (Eq. 8 and 9), our hyperparameter priors took the form

$$
\begin{aligned}
m &\sim \mathcal{N}(\hat{m}, 1)\,, \\
c &\sim \mathcal{N}(\hat{c}, 1)\,, \\
\rho &\sim \ln\mathcal{N}(\ln(\hat{\rho}), 0.1)\,,
\end{aligned}
\tag{20}
$$

where the conventions are the same as above. For our mode amplitudes (Eq. 12 and 13), they took the form

$$
\begin{aligned}
w &\sim \ln\mathcal{N}(\ln(\hat{w}), 10)\,, \\
A &\sim \ln\mathcal{N}(\ln(\hat{A}), 1)\,, \\
V_1 &\sim \ln\mathcal{N}(\ln(\hat{V}_1), 0.1)\,, \\
V_2 &\sim \ln\mathcal{N}(\ln(\hat{V}_2), 0.1)\,, \\
\sigma_A &\sim \mathcal{C}_{1/2}(\beta = 1)\,.
\end{aligned}
\tag{21}
$$

As the convective background had already been fit to our data excluding the region where the modes are present, the results from that fit could be used as extremely informative priors on our fit to the region containing the modes, where there is little information present to constrain the background. To do so, we modeled the background parameters ϕ_B in our full model as being drawn from a multivariate normal distribution as

$$\phi_B \sim \mathcal{N}(\hat{\phi}_B, \underline{\Sigma}_{\hat{\phi}_B}) , \tag{22}$$

where $\hat{\phi}_B$ are the median values of our posterior distributions from our prior background fit, and $\underline{\Sigma}_{\hat{\phi}_B}$ is the full covariance matrix of all the posterior distributions from our prior background fit, taking into account the correlations between the different Harvey components.

Finally, we defined the priors on the rotational parameters: the mode splitting (ν_s), and the inclination angle (i). In order to give these an appropriate treatment, we made two reparameterizations. First, we sampled the projected rotational splitting, $\nu_s \sin(i)$, which is more efficiently sampled due to the strong correlations between i and ν_s [23, 24]. A prior was applied over this as

$$\nu_s \sin(i) \sim \ln \mathcal{N}(\ln(0.75), 0.75) , \tag{23}$$

where conventions are as above. This subjective prior was chosen to reflect that most stars will have a solar-like rotation, with a long tail to allow for the fastest rotators. Second, we sampled in $\cos(i)$, and gave this a prior of

$$\cos(i) \sim \mathcal{U}(0, 1) , \tag{24}$$

which is equivalent to stating that probability to observe an inclination angle i is equal to $\sin(i)$. Here, the $\mathcal{U}(0, 1)$ indicates a uniform prior between 0 and 1. Using a uniform prior on $\cos(i)$ allowed us to account for the geometric effect that stars with a large inclination angle with respect to us are more common [4].

1.5 Fitting procedure

Using our prior information and model described above, we fit Equation 2 to our data $\mathcal{P}$, using the likelihood function described in Section 1.3.

In order to speed up the fitting process, we only applied our model to the region of the power spectrum that contains visible modes of oscillation. We created this subset by removing all frequencies outside a range $0.25 \times \Delta\nu$ below and above the minimum and maximum mode frequencies reported in LEGACY and Kages. This region overlaps minimally with the data used to fit for our prior information of the convective background (see Section 1.4.1), so that both model fits are independent.

To improve computational efficiency, we reduced the number of oscillation modes being fit in five targets. For 16 Cyg A & B, KIC 7970740 and KIC 8478994, we excluded any modes with a Bayes Factor ($\ln(K)$) of less than 6, as reported in LEGACY [5, 6, 25]. For KIC 8478994, which is reported without a value for $\ln(K)$ in Kages, we only included modes of an overtone number that contained a detection for all of $\ell = (0, 1, 2)$, retaining 5 sets of higher
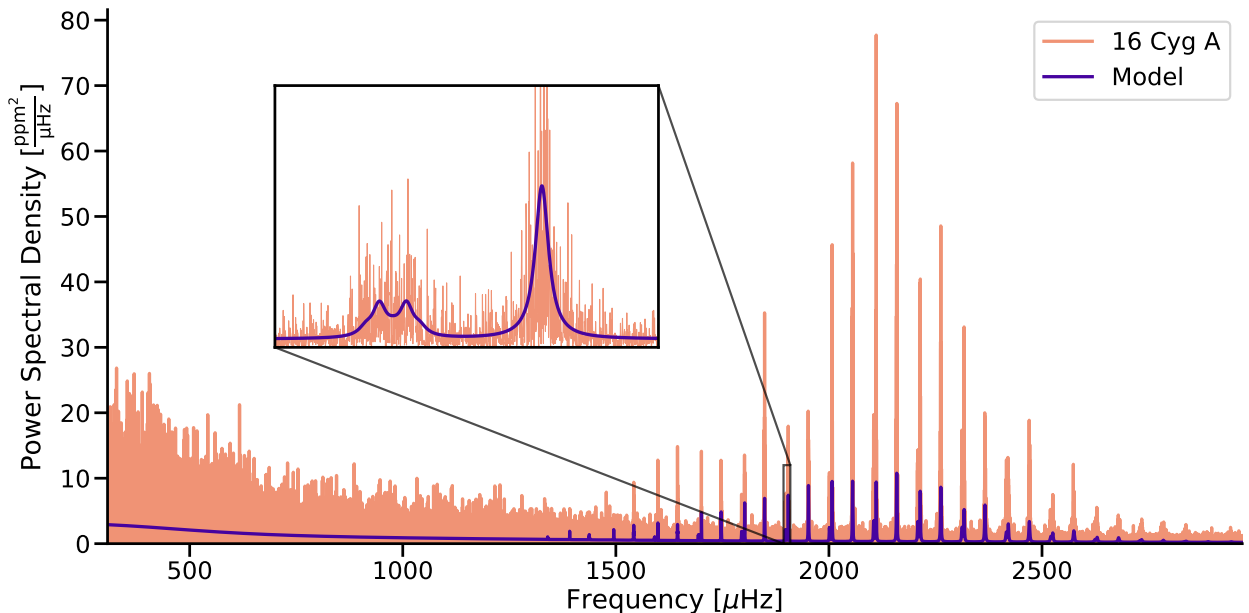
Supplementary Figure 1: A power spectrum constructed from four years of *Kepler* observations of 16 Cyg A (KIC 12069424). Plotted over the top is the model resulting from the fit to the data described in this work. The model implements both the mode frequencies, seen on the right hand side of the plot, and the convective background, the effects of which are seen on the left. Low frequencies have been cropped out for clarity. *Inset*: A zoom in on a radial (right) and quadrupole (left) ($\ell = 0, 2$) pair of modes. The quadrupole mode is split into five components by the star's rotation. Due to the star's inclination angle with respect to us, two out of five peaks are more distinct. The height and spacing of the mode components is a function of the star's rotational splitting ($0.56\,\mu$Hz, equivalent to $P = 20.5$ days) and angle of inclination ($45°$).

signal-to-noise overtones. We do not expect this reduced scope to bias our results, although they may reduce the precision on our measured rotation rates.

We fit our model to our power spectrum data with `PyMC3`, using 2500 iterations each on 4 chains. An example of our model fit to an asteroseismic power spectrum of 16 Cyg A is shown in Supplementary Figure 1.

2 Verifying asteroseismic results

2.1 Priors on rotational parameters

In our Bayesian analysis, we have placed weakly informative priors on our sampled rotational parameters, $\nu_{\rm s}\sin(i)$ and $\cos(i)$. The prior is especially important for the angle of inclination, which is hardest to infer from the data. We are able to validate the robustness of our asteroseismic results by confirming that their posterior distributions are data-dominated, and not prior-dominated. We can do so by comparing the 68% credible regions of the posterior estimates of $\nu_{\rm s}\sin(i)$ and i against the 68% credible regions of their priors.

A comparison between prior and posterior is shown for 94 stars in $\nu_\mathrm{s}\sin(i)$, i and P in Supplementary Figure 2, arranged by age. In the Figure, results with means (symbols) and 68% credible regions (error bars) that are close to those same values for the prior distribution (where the horizontal line is the mean, and the shaded area is the credible region) can be interpreted as prior-dominated (i.e. poorly informed by the data). Cases where the means differ or the credible regions are smaller than the prior distribution are data-dominated. The projected splitting, $\nu_\mathrm{s}\sin(i)$, is overall well constrained, with only one star being prior dominated. This is expected, as the projected splitting is what we observe on the star before decoupling inclination and rotation. The angle of inclination i, sampled as $\cos(i)$, more closely follows the prior distribution in most cases. Combining the two, the rotation period P has no stars directly corresponding to the effective prior on period, and globally follows a trend with increasing age. The three outliers with fast rotation at late ages (KICs 6603624, 8760414 and 8938364) are discussed in more detail in below.

The rotation rates as presented in this work are a product of our Bayesian sampling of both projected splitting and angle of inclination. As seen in the Figure there are instances where i or $\nu_\mathrm{s}\sin(i)$ closely resemble the prior (and are therefore prior-dominated). There are no cases of this when looking at the resulting period measurements, as they will have been informed by at least one strongly data-driven parameter (commonly $\nu_\mathrm{s}\sin(i)$). From this, we concluded that our ensemble of asteroseismic rotation is not strongly dominated by the priors imposed on projected splitting and inclination in our Bayesian analysis.

2.2   Comparisons to previous studies

In order to validate our results, we compared our rotational parameters to those obtained in the literature, as well as those resulting from the work presented in LEGACY and 'Kages', which were unreported and received through private communication by the authors of the catalogue papers.

Comparisons with LEGACY and 'Kages' are shown in Supplementary Figure 3 for projected splitting, inclination angle, and rotation period. In all three cases we show the fractional difference between the values obtained in this work and those from LEGACY and 'Kages'. On the right of the Figure, we show the distribution of the fractional differences for the three parameters. The projected splitting is in good agreement with both studies, however LEGACY finds slightly lower $\nu_\mathrm{s}\sin(i)$ for the faster rotators, deviating from our work by over 1σ. Neither LEGACY nor 'Kages' used a spatially isotropic prior for the inclination angle in their analyses, instead opting for a uniform prior. As posterior estimates of inclination angle are only loosely data-driven, the introduction of an isotropic prior should result in our analysis reporting globally higher inclination angles. This effect is seen in the comparisons of both inclination angles and rotation rates for the LEGACY stars, where we find overall lower rotation rates compared to LEGACY for stars at very similar $\nu_\mathrm{s}\sin(i)$.

A number of stars are excluded from Supplementary Figure 3 and compared individually as extreme outliers: KICs 5094751, 6196457, 8349582, 8494142, 8554498, 105114430 and 11133306 all have fast rotation rates ($< 5\,\mathrm{days}$) in 'Kages', but are found to have a broader spread of rotation rates in this work. At similar values for $\nu_\mathrm{s}\sin(i)$, 'Kages' found much lower inclination angles with highly asymmetrical uncertainties. Based on a comparison between the summary statistics of these stars, we concluded that the results found in this work have
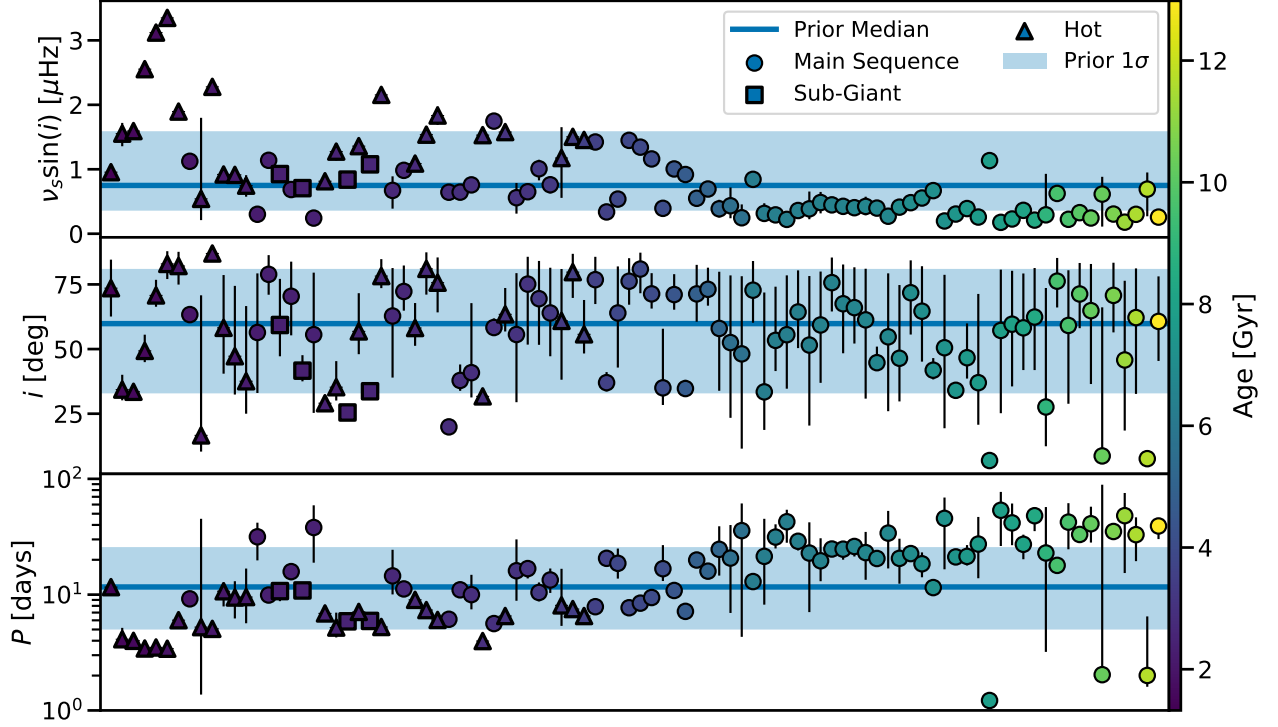
Supplementary Figure 2: **Comparisons between posterior estimates of rotational parameters (data points and error bars) and the priors on these parameters (shaded regions).** The data are sorted from young stars (left) to old (right). Shown are projected splitting ($\nu_{\mathrm{s}}\sin(i)$), inclination angle (i, sampled as $\cos(i)$) and rotation period (P). Both the prior and values for P are a transformation of the upper two parameters (see text). In all cases, the extent of the error bars and shaded regions indicate the 68% credible interval of the posterior and prior distributions respectively. The solid lines indicate the median of the prior distributions. In this figure, results with means and errorbars that closely resemble the prior distribution can be interpreted as prior-dominated (i.e. poorly informed by the data). All stars are sorted and coloured and sorted by age. In the case of inclination angle i and rotation period P, the displayed priors are transformed from the priors imposed on the sampled parameters from which their posteriors were derived.

better marginalised over inclination angle, improving our measure of rotation.

Conversely, KICs 6603624, 8760414 and 8938364 have extremely slow rotation periods in LEGACY, but extremely *fast* (< 3 days) in this work. KICs 8760414 and 8938364 are excluded from the gyrochronology analysis below based on checks for $\hat{R}$ and the number of effective samples. Both stars have ages greater than 10 Gyr, making their fast rotation rates highly unlikely under any model of rotational evolution. The posterior estimate of P for KIC 6603624 is well-defined in our analysis, but with an age of 7.8 Gyr, its measured rotation of 1.2 days is also highly unlikely under any model of rotational evolution. The LEGACY estimate of rotation is similarly extreme at 378 days. These three stars have the lowest inclination angles in our sample ($< 10°$), at which point the power in the split components of the seismic modes is so low that it becomes difficult to probe the measure of splitting. The split components for these stars will have a height roughly 3% of the central mode. For comparison, for the next lowest inclined star at $17°$, this rises to 10%. In cases such as these with lower signal-to-noise, spurious peaks may be interpreted as split components.

We also compared our asteroseismic estimates of stellar rotation with similar studies in the literature, shown in Supplementary Figure 4. These included: a study of the binary solar analogues 16 Cyg A & B [1], ; a study of surface and seismic rotation which our catalogue shares 5 stars with [26], ; and an asteroseismic study of differential rotation with which our catalogue shares 40 targets [27]. For the latter, we used their reported splitting value a_1, which is equivalent to ν_s.

Overall, Supplementary Figure 4 shows no strong disagreements between our asteroseismic measurements for stellar rotation and those from the literature. The scatter of the fractional differences lies cleanly around the zero line, with a mean and spread of $0.0^{+16.4}_{-15.6}$ %. The increase in uncertainty with period is due to more slowly rotating stars being more difficult to constrain using asteroseismology.

It is of note that 16 Cyg A was found to be rotating slightly faster in our analysis compared to the literature [1] (deviating within 2σ), despite the fit being performed on the same data. We found an inclination angle that is slightly lower for 16 Cyg A but at a similar projected splitting, which would explain finding a lower value of rotation.

There are three outliers at low period in Supplementary Figure 4: KICs 6603624, 8760414 and 8938364. These are the same targets found to be outliers in a comparison to the LEGACY and 'Kages' measurements (see above), with anomalously fast rotation rates and low inclination angles. As these stars represent the lowest inclination angles in our sample, and were found to disagree with two independent studies, we opted to exclude them from the gyrochronology analysis, and to flag the rotation measurements for these three stars presented in this work.

2.3 Seismic vs spectroscopic rotation

A distinct difference between rotation rates obtained through different techniques may hold information about differential rotation (both latitudinal and radial) of near-surface layers, such as those we observe in the Sun [28]. A previous comparison of spectroscopic and seismic rotation rates, performed on a sample of 22 stars, found no significant radial differential rotation [27]. In this work they not only considered rotation rates from spots, but also
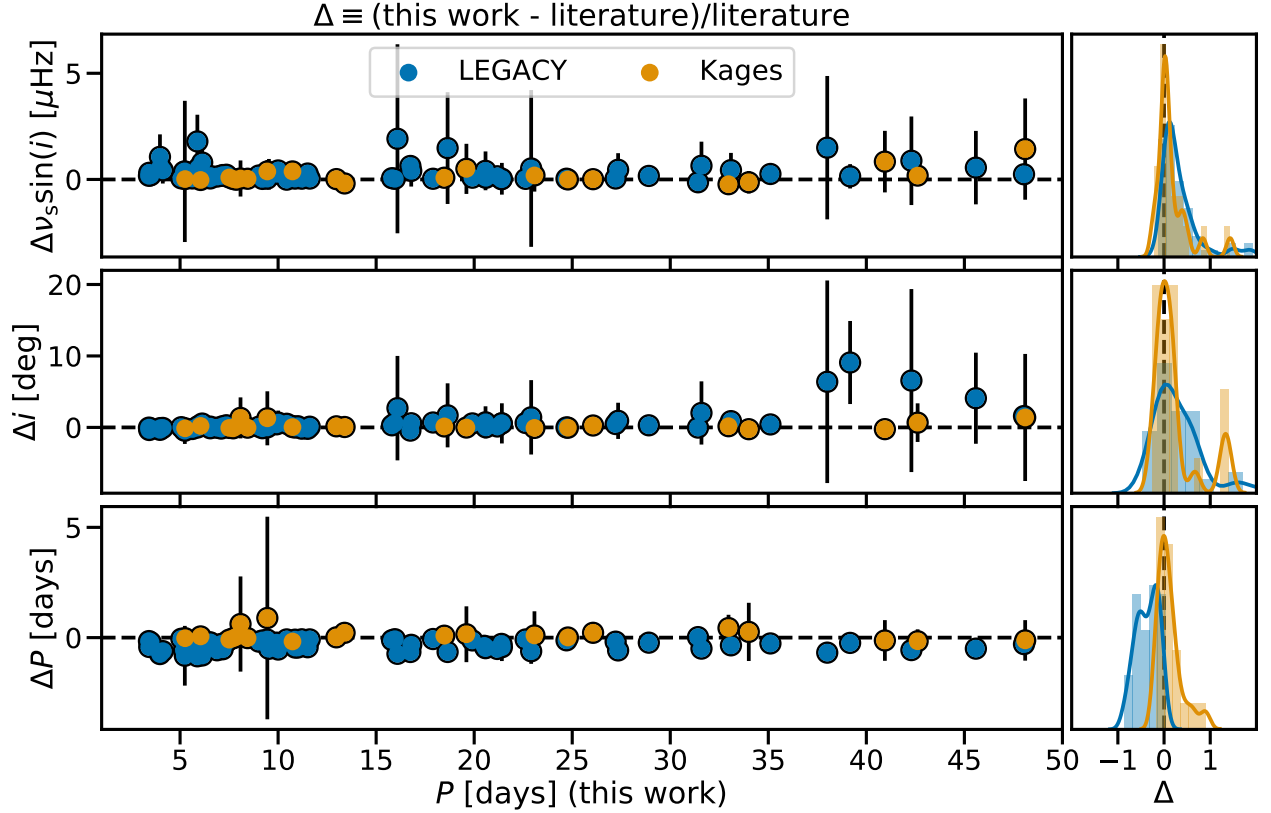
Supplementary Figure 3: **Comparisons between posterior estimates of rotational parameters from this work and the literature**. Literature values are taken from LEGACY and 'Kages' [5, 6, private communication]. Shown are projected splitting ($\nu_s \sin(i)$), inclination angle (i, sampled as $\cos(i)$) and rotation period (P). Fractional differences are plotted against stellar rotation obtained in this work. The Δ indicates the fractional difference between this work and the literature (i.e. stars above the zero-line have higher values in this work). The right hand panels the distribution of the fractional differences around the zero line. The colour legend is consistent throughout all panels. The x-axis units on the right hand panels are equivalent to the y-axis of the left hand panels. 10 stars have been omitted from this plot and are discussed in more detail in the text: KICs 5094751, 6196457, 8349582, 8494142, 8554498, 105114430 and 11133306 all have extremely low rotation periods in Kages, with high uncertainties. Conversely, KICs 6603624, 8760414 and 8938364 have extremely high rotation periods in LEGACY with low uncertainties. Error bars represent the 68% confidence intervals. In cases where stars had asymmetric error bars, the larger of the two was used when propagating uncertainty for the purposes of this figure.

spectroscopic measures of the projected surface rotation $v \sin(i)$, which they found to be more reliable.

With our expanded sample of asteroseismic rotation we can perform a similar analysis, to both validate our sample and probe radial differential rotation. Supplementary Figure 5 shows a comparison between spectroscopic $v \sin(i)$ measurements as listed in LEGACY and 'Kages' (left) and Benomar et al. (2015) [29] (right). In these cases the asteroseismic $v \sin(i)$
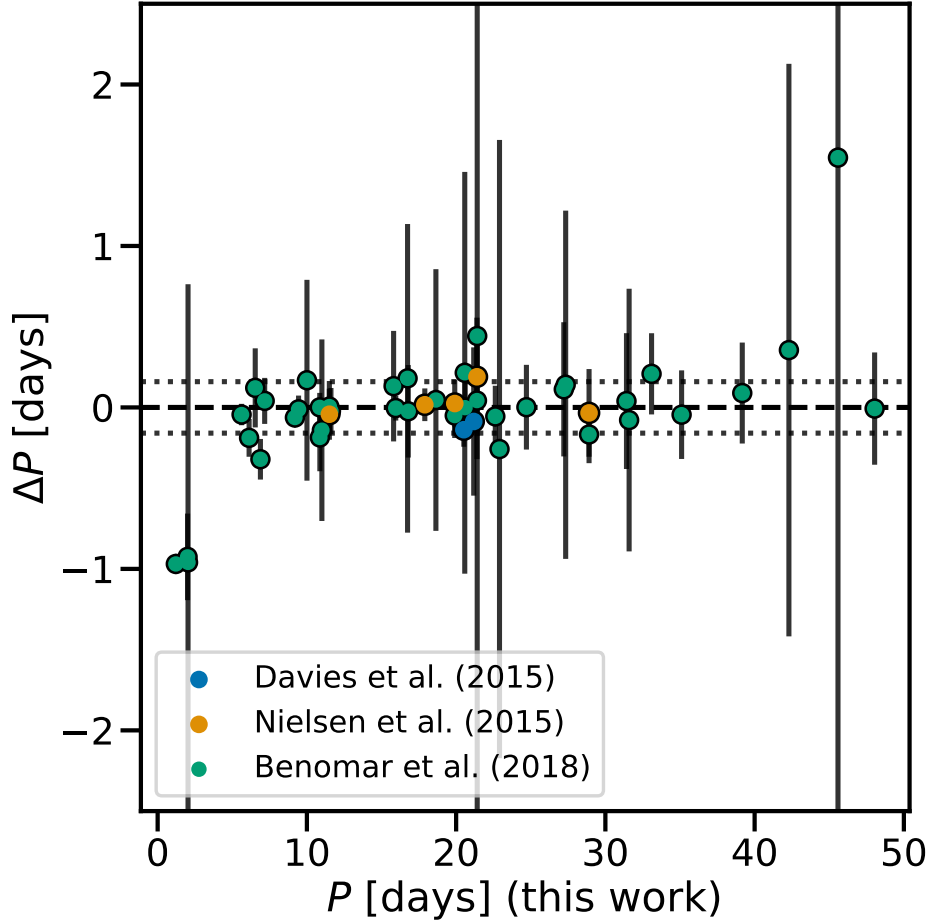
Supplementary Figure 4: **Fractional differences between posterior estimates of aster-oseismic rotation period from this work.** Literature sources are: Davies et al. (2015) [1] (16 Cyg A & B), Nielsen et al. (2015) [26] (5 stars) and Benomar et al. (2018) [27] (40 stars). We used the reported parameter a_1 from the latter, which represents the rotational splitting in the case of uniform latitudinal rotation in their model. The dashed line represents the median of the sample shown, with the dotted lines representing the 15.9th and 84.1st percentiles. Error bars represent the 68% confidence intervals. In cases where stars had asymmetric error bars, the larger of the two was used when propagating uncertainty for the purposes of this figure.

has been calculated using our measure of asteroseismic $\nu_s \sin(i)$ and the known asteroseismic radii. Three stars (KICs 6603624, 8760414 and 8938364) have been excluded from this figure due to strong disagreements of measured rotation rates with the literature (see above).

For the LEGACY and 'Kages' sample, we find no strong deviation from the 1:1 line except at very low velocities, which is likely due to biases inherent to spectroscopic line broadening measurements [30, 31]. For the Benomar et al. (2015) sample stars lie a lot closer to the 1:1 line.

Overall, there appears to be a global offset where spectroscopic measurements of projected

rotation appear faster than asteroseismic measures. Based on the LEGACY and 'Kages' $v\sin(i)$ values, this offset is roughly 18% (i.e. spectroscopic projected rotation rates are faster than asteroseismic rates). This offset is much smaller ($\sim 5\%$) for the [29] sample, albeit for far fewer stars. These offsets are within the typical disagreement between spectroscopic methods, based on comparisons of projected rotation measurements for red giant stars [31, see Figure 2], especially at $< 5\,\mathrm{km\,s^{-1}}$.

It is worth addressing the impact this comparison would have on our conclusions for gyrochronology, were we to take the spectroscopic rotation rates as if they were the truth, even at velocities of $< 5\,\mathrm{km\,s^{-1}}$. For the majority of cases, the seismic velocities are slower than the spectroscopic velocities, which would bias our ensemble towards favouring a standard evolution over a weakened magnetic braking scenario (as stars would overall appear to be rotating slower at late ages). Based on the comparison to spot rotation presented in the main body of this paper, and given known issues comparing seismic and spectroscopic rotation at low velocities, we concluded that the divergence seen in Supplementary Figure 5 does not undermine our results.
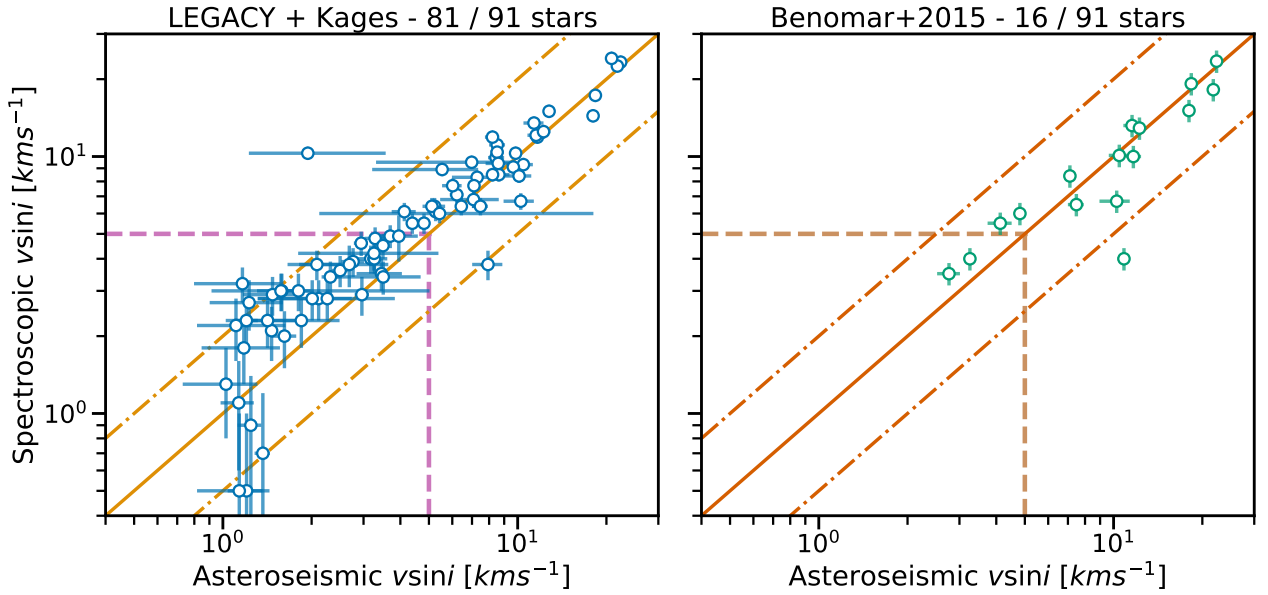
Supplementary Figure 5: **Comparisons between asteroseismic and spectroscopic measures of projected surface rotation, $v\sin(i)$.** All asteroseismic (x-axis) values are from this work, all spectroscopic (y-axis) values are from the literature. *Left*: comparisons to 81 stars values reported in LEGACY and Kages. *Right*: comparisons to 16 stars observed by Benomar et al. (2015) [29]. Asteroseismic values are transformed from projected splitting ($\nu_s \sin(i)$) using the asteroseismic radius measurements presented in LEGACY and 'Kages'. Horizontal error bars represent the 68% confidence intervals. Vertical error bars represent the formal uncertainty on the published spectroscopic values. The solid lines indicate the 1:1 line, while the dash-dotted lines represent the 2:1 and 1:2 lines. The dashed lines indicate the location of $v\sin(i) = 5\,\mathrm{km s^{-1}}$, the point at which surface and seismic measures of projected rotation begin to differ strongly [31].

2.4 Asteroseismic detection biases

Stars that are rotating very slowly will show small rotational splittings, which may be indistinguishable from a non-rotating case, wheras stars that are spinning very fast may find that their splitting is so wide that they cross over with split modes at different radial orders (n). Asteroseismic selection techniques may also introduce additional biases on a population level. We consider the limitations this places on our asteroseismic method.

- *Fast rotating stars:* In prinicple, a star could rotate fast enough that the highest-frequency peak in a split dipole ($\ell = 2$) mode would overlap with the radial ($\ell = 0$) mode. This would occur if $2\nu_\mathrm{s} > \delta\nu_{02}$, the small separation. For the star in our sample with the smallest $\delta\nu_{02}$ (so the highest risk of this happening), this would occur at a rotation of 8.8 days or faster. For the star with the largest $\delta\nu_{02}$, this limit was roughly 2 days.

  In practice, the model still properly fits a spectrum where this kind of mode-overlapping occurs, as the $\ell = 0$ modes don't split, meaning that there are no degenerate solutions in this regime, and further constraints can be obtained from the other modes and split components in the spectrum. A more serious issue may be when the $\ell = 1$ mode at lower frequencies overlaps with the $\ell = 2$ mode as well, which would only occur at a rotation rate of 2 days or faster for the star with the smallest $\delta\nu_{01}$.

- *Slow rotating stars:* Except for the most rapidly rotating cases, asteroseismic mode splitting is detected by a change in the distribution of the power of mode frequencies as the split components begin to separate from the central mode. If there is to be hard limit at which this measurement is not possible, it should be in the case that $\nu_\mathrm{s} < 2/T$, where T is the observation time, and $1/T$ is the frequency bin width. For the star in our sample with the shortest observing time, this limit would be ~ 89 days, which quickly rises for longer observing baselines. While this constitutes a hard limit, slower rotation rates will become harder and harder to constrain as the rate of splitting becomes smaller. A benefit of the Bayesian approach used in this paper is that it should accurately reflect the increased uncertainty associated with the small rotational splitting.

While these two limits cause concern when studying the most extreme rotators, the results presented in this work are driven by stars with rotation rates in the regime of 5 to 30 days. Above, we demonstrated that results on period for these stars were data-driven (i.e. do not reflect the priors), indicating that the splitting is well resolved in this regime, and so we do not expect these limits to bias our conclusions.

Finally, we also consider bias in asteroseismic detections. The probability of an asteroseismic detection with *Kepler* scales with temperature and radius (i.e. scales inversely with $\log(g)$, and therefore main sequence age), and detections are unlikely below roughly $5200\,K$ [2, 32]. Very young ($\lesssim 2\,\mathrm{Gyr}$), very magnetically active stars may also suppress their oscillation modes. [33]. Though these two effects impose a bias on asteroseismic populations, they do so outside the parameter range on which our comparison takes place. As it is older stars, undergoing magnetic braking, that are required to drive the distinction between stellar models, we conclude that our seismic sample can be assumed to be complete for the purposes of this work.

3 Verifying consequences for gyrochronology

3.1 Limits of our stellar models

The rotational stellar models used in this work [34] are constructed for metallicities of $-0.4 <$ [Fe/H] < 0.4 dex, in steps of 0.1 dex. Our sample of 91 stars contained 4 stars with metallicities below -0.4 dex, which are shown as shaded symbols in Figure **??**. Of these, 3 were included in our final sample of 73 stars used to evaluate our stellar models: KICs 7970740, 8684723 and KIC 9965715. All three are classed as MS stars, with metallicities of -0.54 ± 0.10, -0.42 ± 0.10 and -0.44 ± 0.18 dex respectively, placing them within 3σ of the metallicity limits of our stellar models. KICs 8684723 and 9965715 strongly agree with the WMB model, whereas KIC 7970740 weakly prefers the standard model. Excluding these stars was not found to significantly alter the joint posterior distribution shown in Figure 4 of the main paper.

A recent study [35] compared different rotational evolution models [36, 37, of which we use the former in this work] while studying the effect metallicity has on rotation. They found that metal-rich stars spin down significantly more effectively than metal poor stars. The population of 73 stars used in our stellar model comparisons is roughly centered on a [Fe/H] of 0 dex, with a spread of 0.16 dex, with no stars significantly above or below ± 0.4 dex (as discussed above). While differences in stellar rotational evolution as a function of metallicity in this region are still somewhat pronounced, they are much less so than for more metal-rich or poor stars [35, see Figure 2]. However, for stars with [Fe/H] < 0, the alternative model prescription [37] sees stars spin down more slowly than the models used in this work (i.e. they will rotate faster at later ages). This work only explores the presence of weakened magnetic braking for a single braking law, and a comparison to alternative braking model will be explored in a future paper.

When constructing KDEs from our stellar model samples (see Section **??**), we selected fixed resolutions (or band-widths) for the KDEs. In mass, the band-width of $0.02 \odot$, was larger than the uncertainties of 24 of 73 stars used to construct our joint posterior. For the stars with the smallest uncertainties, this significantly limits the size of the KDE being evaluated (as subsections of the full stellar models are used to evaluate individual stars, for computational efficiency). In order to confirm that these stars do not significantly affect the ensemble's preference towards the WMB model, we recalculated the joint posterior distribution for Q_{WMB}, excluding stars with an uncertainty on mass smaller than the KDE band-width. While the 24 stars with small uncertainties do favour the WMB model, they do so very weakly, whereas the remaining 49 stars with larger uncertainties strongly favour the WMB model. Their removal from the total joint posterior probability does not significantly alter it from the distribution shown in Figure 4 of the main paper.

3.2 Systematic uncertainties from asteroseismology

In our model analysis, we used asteroseismic mass and age obtained using `BASTA`, as reported in LEGACY and Kages. Asteroseismic properties obtained through stellar models can be subject to systematic errors arising from differences in input physics and choice of stellar models not included in the reported statistical uncertainties. A quantification of these different systematic effects can be found in the 'Kages' catalogue paper [38]. Combining their reported

median systematic uncertainties due to input physics results in median uncertainties of 20% (up from 14%) on age and 5% (up from 3%) on mass for the 'Kages' sample. For LEGACY, the median uncertainties are 18% (up from 10%) and 5.6% (up from 4%) for age and mass respectively.

We re-ran our model analysis after inflating uncertainties on mass and age. We increased uncertainties by the fractional difference between the BASTA statistical uncertainties and the median full statistical and systematic uncertainties described above. For example, a LEGACY star with a mass of $2.0 \pm 0.5\,M_\odot$ would have its uncertainty inflated by 1.6% of its mass, to $0.53\,M_\odot$.

To further test the limits of this analysis, we also reran our mixture model fit, this time only shifting the asteroseismic ages younger by the systematic uncertainty, and retaining the statistical uncertainty (i.e. the ages of LEGACY and 'Kages' stars were reduced by 8% and 6% respectively). In this scenario where all asteroseismic ages are overestimated, 'true' fast rotators at young ages would have been mistaken for fast rotators at old ages, suggesting the presence of weakened magnetic braking where none existed.

The results of these tests are discussed further in the main body of the paper.

3.3   Binaries and Planet Hosts

For stars to be good probes of existing gyrochronology relations, their rotational evolution must occur in isolation. If a star interacts with a close binary companion (through tides, or a merger) the natural angular momentum loss can be disturbed, causing gyrochronology to mispredict ages [39, 40]. Between LEGACY and Kages, we have 8 known binaries.

First, KIC 8379927, KIC 7510397, KIC 10454113 and KIC 9025370 are spectroscopic binaries. This does not affect the asteroseismic analysis, but may affect their rotational evolution. Of these, KICs 8379927, 7510397 and 9025370 were included in the gyrochronology analysis. None of them preferred one model strongly over the other, with all three finding flat posteriors for Q_{WMB}.

Second, the binary pairs of KIC 9139151 & 9139163 and 16 Cyg A & B are individually observed binary components with wide orbital separations, so we do not expect their binarity to have affected their rotational evolution [41, 42].

While we chose not to account for star-planet tidal interactions in this work, we note that this may disturb the natural stellar rotational evolution when tidal forces are at play [43, 44, 45], although this has been disputed by observations of asteroseismic planet hosts [46].

4   Supplementary Table

Table 1: Parameters for the 94 stars for which seismic rotation rates were obtained in this work. Temperature ($T_{\rm eff}$), age, mass, metallicity ([Fe/H]) and surface gravity ($\log(g)$) are adopted from the LEGACY [6, 47, L] and 'Kages' [38, 5, K] catalogues, as listed in the Source column. Projected splitting ($\nu_{\rm s}\sin(\hat{i})$), inclination angle ($\hat{i}$) and asteroseismic rotation (P) are from this work. Uncertainties were taken using the 15.9$^{\rm th}$ and 84.1$^{\rm st}$ percentiles of posterior distributions on the parameters, which are frequently asymmetrical in linear space. Reported values are the median of the posteriors. For parameters with no direct posterior samples (e.g. rotation) the full posterior samples were transformed before taking the summary statistics. The stellar type denotes whether a star is roughly classified as belonging to the main sequence (MS), Sub-Giants (SG) or 'hot' stars (H) (see text). The flags indicate the following: 0; no issues, used in the gyrochronology analysis. 1; has either a number of effective samples $n_{\rm eff} < 1000$ for the asteroseismic splitting, or Gelman-Rubin convergence metric of $\hat{R} > 1.1$ [?], indicating that rotation measurements for these stars are less robust than those with a flag of 0. 2; was found to strongly disagree with multiple literature values, excluded from the gyrochronology analysis. 3; fell outside the model range of the stellar models, and were therefore not used in the gyrochronology analysis. Table is continued on next page.

KIC	$T_{\rm eff}$ [K]	Age [Gyr]	Mass [M$_\odot$]	[Fe/H] [dex]	$\log(g)$ [dex]	$\nu_{\rm s}\sin(\hat{i})$ [μHz]	$\hat{i}$ [°]	P [days]	Flag	Type	Source
1435467	6326±77	$3.02^{+0.50}_{-0.35}$	$1.32^{+0.03}_{-0.05}$	0.01±0.10	$4.100^{+0.009}_{-0.009}$	$1.58^{+0.10}_{-0.09}$	$63.4^{+10.2}_{-6.6}$	$6.5^{+0.8}_{-0.8}$	0	H	L
2837475	6614±77	$1.63^{+0.11}_{-0.11}$	$1.43^{+0.02}_{-0.05}$	0.01±0.10	$4.163^{+0.007}_{-0.007}$	$3.12^{+0.08}_{-0.08}$	$70.7^{+6.6}_{-6.0}$	$3.5^{+0.2}_{-0.2}$	0	H	L
3425851	6343±85	$3.32^{+0.85}_{-0.85}$	$1.18^{+0.05}_{-0.05}$	-0.04±0.10	$4.243^{+0.008}_{-0.008}$	$1.17^{+0.48}_{-0.48}$	$60.9^{+20.1}_{-22.7}$	$8.1^{+8.6}_{-2.7}$	0	H	K
3427720	6045±77	$2.23^{+0.24}_{-0.24}$	$1.11^{+0.02}_{-0.01}$	-0.06±0.10	$4.387^{+0.005}_{-0.004}$	$0.30^{+0.06}_{-0.06}$	$56.4^{+22.9}_{-23.4}$	$31.6^{+10.2}_{-11.8}$	0	MS	L
3456181	6384±77	$2.09^{+0.13}_{-0.13}$	$1.50^{+0.02}_{-0.02}$	-0.15±0.10	$3.949^{+0.009}_{-0.008}$	$0.92^{+0.08}_{-0.08}$	$58.2^{+20.4}_{-17.7}$	$10.7^{+2.0}_{-2.8}$	0	H	L
3544595	5669±75	$6.63^{+0.62}_{-0.57}$	$0.90^{+0.01}_{-0.01}$	-0.18±0.10	$4.468^{+0.003}_{-0.003}$	$0.40^{+0.04}_{-0.04}$	$66.0^{+15.6}_{-13.9}$	$26.1^{+3.9}_{-4.7}$	0	MS	K
3632418	6193±77	$2.63^{+0.18}_{-0.18}$	$1.41^{+0.02}_{-0.02}$	-0.12±0.10	$4.024^{+0.008}_{-0.008}$	$0.98^{+0.03}_{-0.03}$	$72.3^{+10.0}_{-7.4}$	$11.2^{+0.6}_{-0.7}$	0	MS	L
3656476	5668±77	$8.37^{+1.57}_{-1.54}$	$1.04^{+0.04}_{-0.05}$	0.25±0.10	$4.225^{+0.008}_{-0.008}$	$0.21^{+0.02}_{-0.02}$	$62.4^{+18.9}_{-20.5}$	$48.0^{+8.1}_{-12.7}$	0	MS	L
3735871	6107±77	$2.35^{+0.85}_{-0.85}$	$1.09^{+0.04}_{-0.04}$	-0.04±0.10	$4.396^{+0.007}_{-0.007}$	$0.69^{+0.05}_{-0.05}$	$70.4^{+13.4}_{-15.1}$	$15.8^{+1.8}_{-2.5}$	0	MS	L
4141376	6134±91	$3.27^{+0.59}_{-0.59}$	$1.02^{+0.02}_{-0.03}$	-0.24±0.10	$4.412^{+0.004}_{-0.003}$	$0.76^{+0.13}_{-0.13}$	$64.0^{+17.5}_{-16.7}$	$13.4^{+3.4}_{-3.0}$	0	MS	K
4143755	5622±106	$11.27^{+1.50}_{-1.35}$	$0.92^{+0.02}_{-0.03}$	-0.40±0.11	$4.102^{+0.002}_{-0.001}$	$0.18^{+0.08}_{-0.05}$	$45.8^{+30.6}_{-27.3}$	$48.1^{+27.4}_{-32.7}$	1	MS	K
4349452	6270±79	$3.45^{+0.81}_{-0.72}$	$1.16^{+0.04}_{-0.05}$	-0.04±0.10	$4.275^{+0.008}_{-0.007}$	$1.50^{+0.09}_{-0.09}$	$79.7^{+7.1}_{-10.0}$	$7.5^{+0.5}_{-0.6}$	0	H	K
4914423	5845±88	$6.67^{+0.69}_{-0.62}$	$1.10^{+0.02}_{-0.03}$	0.07±0.11	$4.155^{+0.004}_{-0.004}$	$0.42^{+0.15}_{-0.14}$	$61.3^{+19.8}_{-30.5}$	$23.1^{+11.7}_{-9.6}$	0	MS	K
4914923	5805±77	$7.57^{+1.66}_{-1.79}$	$1.06^{+0.06}_{-0.05}$	0.08±0.10	$4.197^{+0.008}_{-0.008}$	$0.39^{+0.03}_{-0.03}$	$46.6^{+13.3}_{-8.1}$	$21.4^{+5.4}_{-3.5}$	0	MS	L
5094751	5952±75	$6.35^{+1.05}_{-1.05}$	$1.07^{+0.04}_{-0.04}$	-0.08±0.10	$4.213^{+0.008}_{-0.007}$	$0.39^{+0.27}_{-0.16}$	$51.5^{+26.7}_{-31.1}$	$22.9^{+19.3}_{-15.8}$	0	MS	K
5184732	5846±77	$4.85^{+1.57}_{-0.88}$	$1.15^{+0.04}_{-0.06}$	0.36±0.10	$4.255^{+0.010}_{-0.008}$	$0.55^{+0.02}_{-0.02}$	$71.3^{+11.2}_{-10.8}$	$19.9^{+1.3}_{-1.9}$	0	MS	L
5773345	6130±84	$2.55^{+0.26}_{-0.24}$	$1.47^{+0.03}_{-0.03}$	0.21±0.09	$3.993^{+0.008}_{-0.007}$	$1.08^{+0.08}_{-0.08}$	$33.7^{+2.8}_{-2.5}$	$5.9^{+0.7}_{-0.5}$	0	SG	L
5866724	6169±50	$3.89^{+0.59}_{-0.48}$	$1.20^{+0.03}_{-0.03}$	0.09±0.08	$4.224^{+0.005}_{-0.007}$	$1.34^{+0.08}_{-0.07}$	$80.9^{+6.3}_{-9.4}$	$8.4^{+0.5}_{-0.5}$	0	MS	K
5950854	5853±77	$8.93^{+1.12}_{-1.15}$	$0.97^{+0.03}_{-0.03}$	-0.23±0.10	$4.238^{+0.007}_{-0.007}$	$0.29^{+0.64}_{-0.12}$	$27.6^{+46.0}_{-15.2}$	$22.9^{+34.2}_{-19.7}$	1	MS	L

Continued on next page

19

Table 1: *Continued from previous page.*

KIC	$T_{\rm eff}$ [K]	Age [Gyr]	Mass [$M_\odot$]	[Fe/H] [dex]	$\log(g)$ [dex]	$\nu_{\rm s}\sin(i)$ [μHz]	i [°]	P [days]	Flag	Type	Source
6106415	6037±77	$5.03^{+1.28}_{-1.12}$	$1.07^{+0.05}_{-0.04}$	-0.04 ± 0.10	$4.295^{+0.009}_{-0.009}$	$0.69^{+0.02}_{-0.02}$	$73.1^{+8.4}_{-6.3}$	$16.0^{+0.7}_{-0.8}$	0	MS	L
6116048	6033±77	$9.58^{+2.16}_{-1.90}$	$0.94^{+0.05}_{-0.05}$	-0.23 ± 0.10	$4.254^{+0.009}_{-0.009}$	$0.63^{+0.02}_{-0.02}$	$76.3^{+9.0}_{-10.2}$	$17.9^{+0.8}_{-0.8}$	0	MS	L
6196457	5871±94	$5.52^{+0.51}_{-1.90}$	$1.21^{+0.02}_{-0.05}$	0.17 ± 0.11	$4.049^{+0.005}_{-0.005}$	$0.43^{+0.28}_{-0.19}$	$52.5^{+26.0}_{-29.1}$	$20.7^{+19.2}_{-13.7}$	0	MS	K
6225718	6313±76	$2.41^{+0.53}_{-0.43}$	$1.16^{+0.03}_{-0.03}$	-0.07 ± 0.10	$4.319^{+0.005}_{-0.007}$	$0.81^{+0.03}_{-0.03}$	$29.1^{+2.1}_{-1.8}$	$6.9^{+0.6}_{-0.5}$	0	H	L
6278762	5046±74	$11.54^{+0.99}_{-0.94}$	$0.74^{+0.01}_{-0.01}$	-0.37 ± 0.09	$4.560^{+0.002}_{-0.003}$	$0.30^{+0.09}_{-0.09}$	$62.2^{+19.0}_{-29.5}$	$33.0^{+13.6}_{-13.5}$	1, 3	MS	K
6508366	6331±77	$2.06^{+0.14}_{-0.13}$	$1.53^{+0.02}_{-0.02}$	-0.05 ± 0.10	$3.942^{+0.007}_{-0.007}$	$2.28^{+0.04}_{-0.04}$	$87.0^{+2.1}_{-3.2}$	$5.1^{+0.1}_{-0.1}$	0	H	L
6521045	5825±75	$6.50^{+0.46}_{-0.56}$	$1.11^{+0.02}_{-0.02}$	0.02 ± 0.10	$4.125^{+0.004}_{-0.004}$	$0.45^{+0.03}_{-0.02}$	$75.7^{+9.7}_{-11.2}$	$24.8^{+1.9}_{-2.0}$	0	MS	K
6603624	5674±77	$7.82^{+0.94}_{-0.94}$	$1.01^{+0.03}_{-0.03}$	0.28 ± 0.10	$4.320^{+0.004}_{-0.005}$	$1.13^{+0.13}_{-0.13}$	$6.9^{+0.8}_{-0.8}$	$1.2^{+0.0}_{-0.0}$	2	MS	L
6679371	6479±77	$1.95^{+0.18}_{-0.16}$	$1.53^{+0.04}_{-0.04}$	0.01 ± 0.10	$3.934^{+0.007}_{-0.008}$	$1.90^{+0.05}_{-0.06}$	$82.1^{+5.5}_{-7.2}$	$6.0^{+0.2}_{-0.2}$	0	H	L
6933899	5832±77	$6.34^{+0.72}_{-0.62}$	$1.13^{+0.03}_{-0.03}$	-0.01 ± 0.10	$4.087^{+0.008}_{-0.007}$	$0.36^{+0.02}_{-0.02}$	$64.3^{+16.1}_{-14.0}$	$28.9^{+3.7}_{-4.8}$	0	MS	L
7103006	6344±77	$2.47^{+0.22}_{-0.24}$	$1.42^{+0.04}_{-0.02}$	0.02 ± 0.10	$4.015^{+0.007}_{-0.007}$	$1.36^{+0.08}_{-0.09}$	$56.8^{+14.8}_{-8.8}$	$7.1^{+1.3}_{-1.0}$	0	H	L
7106245	6068±102	$6.27^{+1.06}_{-1.06}$	$0.92^{+0.04}_{-0.03}$	-0.99 ± 0.19	$4.325^{+0.008}_{-0.007}$	$0.32^{+0.16}_{-0.10}$	$33.4^{+23.8}_{-14.7}$	$21.4^{+23.8}_{-13.2}$	1, 3	MS	L
7206837	6305±77	$2.90^{+0.42}_{-0.30}$	$1.30^{+0.03}_{-0.03}$	0.10 ± 0.10	$4.163^{+0.007}_{-0.008}$	$1.53^{+0.12}_{-0.12}$	$31.7^{+3.2}_{-2.8}$	$4.0^{+0.6}_{-0.4}$	0	H	L
7296438	5775±77	$7.23^{+1.49}_{-1.45}$	$1.08^{+0.06}_{-0.06}$	0.19 ± 0.10	$4.201^{+0.009}_{-0.010}$	$0.20^{+0.06}_{-0.06}$	$50.5^{+31.1}_{-29.0}$	$45.6^{+23.4}_{-29.0}$	1	MS	L
7510397	6171±77	$2.82^{+0.14}_{-0.16}$	$1.37^{+0.02}_{-0.02}$	-0.21 ± 0.10	$4.036^{+0.007}_{-0.004}$	$0.64^{+0.06}_{-0.06}$	$19.9^{+2.0}_{-2.0}$	$6.1^{+0.7}_{-0.6}$	0	MS	L
7670943	6463±110	$2.78^{+0.62}_{-0.51}$	$1.24^{+0.04}_{-0.05}$	0.09 ± 0.11	$4.228^{+0.008}_{-0.008}$	$1.83^{+0.14}_{-0.14}$	$75.7^{+9.8}_{-11.5}$	$6.0^{+0.6}_{-0.6}$	0	H	K
7680114	5811±77	$7.68^{+1.45}_{-1.28}$	$1.06^{+0.03}_{-0.05}$	0.05 ± 0.10	$4.172^{+0.008}_{-0.010}$	$0.26^{+0.05}_{-0.04}$	$37.0^{+34.3}_{-16.3}$	$27.3^{+19.6}_{-13.5}$	0	MS	L
7771282	6248±77	$3.24^{+0.35}_{-0.32}$	$1.29^{+0.03}_{-0.03}$	-0.02 ± 0.10	$4.112^{+0.007}_{-0.007}$	$1.01^{+0.14}_{-0.18}$	$69.5^{+17.8}_{-14.6}$	$10.4^{+2.3}_{-1.7}$	0	MS	L
7871531	5501±77	$9.96^{+1.93}_{-1.77}$	$0.83^{+0.03}_{-0.02}$	-0.26 ± 0.10	$4.478^{+0.005}_{-0.007}$	$0.33^{+0.03}_{-0.03}$	$71.3^{+12.0}_{-13.2}$	$33.1^{+4.1}_{-4.1}$	0	MS	L
7940546	6235±77	$2.33^{+0.08}_{-0.08}$	$1.40^{+0.03}_{-0.01}$	-0.20 ± 0.10	$4.007^{+0.003}_{-0.005}$	$1.14^{+0.03}_{-0.03}$	$78.9^{+7.4}_{-7.9}$	$9.9^{+0.3}_{-0.4}$	0	MS	L
7970740	5309±77	$12.98^{+1.36}_{-2.00}$	$0.73^{+0.03}_{-0.03}$	-0.54 ± 0.10	$4.539^{+0.004}_{-0.005}$	$0.26^{+0.03}_{-0.02}$	$60.7^{+17.4}_{-15.3}$	$39.2^{+6.7}_{-9.0}$	0	MS	L
8006161	5488±77	$3.59^{+1.53}_{-1.45}$	$0.98^{+0.03}_{-0.03}$	0.34 ± 0.10	$4.494^{+0.007}_{-0.007}$	$0.34^{+0.02}_{-0.02}$	$37.0^{+4.1}_{-3.4}$	$20.6^{+1.8}_{-2.2}$	0	MS	L
8077137	6072±75	$6.23^{+1.23}_{-1.23}$	$1.12^{+0.05}_{-0.05}$	-0.09 ± 0.10	$4.056^{+0.010}_{-0.013}$	$0.84^{+0.06}_{-0.07}$	$72.8^{+11.3}_{-12.6}$	$13.0^{+1.3}_{-1.5}$	0	MS	K
8150065	6173±101	$3.83^{+0.99}_{-0.67}$	$1.19^{+0.04}_{-0.05}$	-0.13 ± 0.15	$4.220^{+0.008}_{-0.008}$	$0.54^{+0.11}_{-0.13}$	$64.0^{+18.0}_{-21.1}$	$18.6^{+6.4}_{-4.9}$	0	MS	L
8179536	6343±77	$3.54^{+1.04}_{-1.04}$	$1.16^{+0.05}_{-0.06}$	-0.03 ± 0.10	$4.255^{+0.007}_{-0.010}$	$1.46^{+0.09}_{-0.10}$	$55.7^{+13.3}_{-7.4}$	$6.5^{+1.2}_{-1.2}$	0	H	L
8228742	6122±77	$2.89^{+0.18}_{-0.16}$	$1.38^{+0.02}_{-0.02}$	-0.08 ± 0.10	$4.035^{+0.007}_{-0.007}$	$0.64^{+0.04}_{-0.04}$	$37.9^{+6.2}_{-4.9}$	$11.0^{+2.0}_{-1.3}$	0	MS	L
8292840	6239±94	$3.85^{+0.81}_{-0.81}$	$1.15^{+0.05}_{-0.05}$	-0.14 ± 0.10	$4.240^{+0.008}_{-0.008}$	$1.45^{+0.07}_{-0.07}$	$76.2^{+8.9}_{-9.1}$	$7.7^{+0.5}_{-0.5}$	0	MS	K
8349582	5699±74	$8.03^{+0.80}_{-0.70}$	$1.07^{+0.02}_{-0.02}$	0.30 ± 0.10	$4.163^{+0.004}_{-0.003}$	$0.23^{+0.07}_{-0.06}$	$59.6^{+20.7}_{-24.1}$	$41.7^{+19.6}_{-14.9}$	1	MS	K
8379927	6067±120	$1.99^{+0.85}_{-0.75}$	$1.12^{+0.04}_{-0.04}$	-0.10 ± 0.15	$4.388^{+0.008}_{-0.007}$	$1.12^{+0.02}_{-0.02}$	$63.3^{+2.5}_{-2.3}$	$9.2^{+0.3}_{-0.2}$	0	MS	L
8394589	6143±77	$4.45^{+0.94}_{-0.83}$	$1.04^{+0.03}_{-0.03}$	-0.29 ± 0.10	$4.322^{+0.008}_{-0.008}$	$1.01^{+0.03}_{-0.03}$	$71.1^{+7.9}_{-5.9}$	$10.9^{+0.6}_{-0.6}$	0	MS	L
8424992	5719±77	$9.61^{+1.92}_{-1.74}$	$0.92^{+0.04}_{-0.04}$	-0.12 ± 0.10	$4.359^{+0.005}_{-0.007}$	$0.22^{+0.06}_{-0.06}$	$59.1^{+21.3}_{-30.3}$	$42.3^{+19.4}_{-17.7}$	1	MS	L
8494142	6144±106	$2.62^{+0.26}_{-0.45}$	$1.42^{+0.03}_{-0.03}$	0.13 ± 0.10	$4.038^{+0.005}_{-0.003}$	$0.67^{+0.22}_{-0.21}$	$62.8^{+23.8}_{-18.5}$	$14.5^{+9.9}_{-4.5}$	0	MS	K
8554498	5945±60	$5.60^{+0.45}_{-0.42}$	$1.20^{+0.02}_{-0.03}$	0.17 ± 0.05	$4.007^{+0.003}_{-0.003}$	$0.25^{+0.09}_{-0.09}$	$48.1^{+25.6}_{-36.6}$	$35.7^{+25.6}_{-31.4}$	0	MS	K

Continued on next page

Table 1: *Continued from previous page.*

KIC	$T_{\rm eff}$ [K]	Age [Gyr]	Mass [M$_\odot$]	[Fe/H] [dex]	$\log(g)$ [dex]	$\nu_{\rm s}\sin(i)$ [μHz]	i [°]	P [days]	Flag	Type	Source
8694723	6246 ± 77	$4.69^{+0.48}_{-0.51}$	$1.14^{+0.02}_{-0.02}$	-0.42 ± 0.10	$4.113^{+0.007}_{-0.007}$	$0.92^{+0.05}_{-0.05}$	$34.7^{+3.4}_{-2.7}$	$7.2^{+0.8}_{-0.8}$	0	MS	L
8760414	5873 ± 77	$11.66^{+1.28}_{-1.61}$	$0.81^{+0.03}_{-0.03}$	-0.92 ± 0.10	$4.329^{+0.006}_{-0.006}$	$0.69^{+0.26}_{-0.42}$	$7.6^{+2.3}_{-1.7}$	$2.0^{+4.5}_{-0.6}$	2, 3	MS	L
8866102	6325 ± 75	$2.60^{+0.56}_{-0.53}$	$1.23^{+0.04}_{-0.04}$	0.01 ± 0.10	$4.262^{+0.008}_{-0.005}$	$2.15^{+0.04}_{-0.04}$	$78.2^{+6.6}_{-4.7}$	$5.3^{+0.2}_{-0.2}$	0	H	K
8938364	5677 ± 77	$10.25^{+0.56}_{-0.65}$	$0.99^{+0.01}_{-0.01}$	-0.13 ± 0.10	$4.173^{+0.007}_{-0.002}$	$0.61^{+0.27}_{-0.50}$	$8.7^{+57.5}_{-2.3}$	$2.0^{+87.0}_{-0.7}$	2	MS	L
9025370	5270 ± 180	$6.55^{+1.26}_{-1.13}$	$0.97^{+0.03}_{-0.03}$	-0.12 ± 0.18	$4.423^{+0.005}_{-0.007}$	$0.43^{+0.04}_{-0.04}$	$67.5^{+15.2}_{-19.1}$	$24.7^{+3.7}_{-4.7}$	0	MS	L
9098294	5852 ± 77	$8.08^{+0.73}_{-0.99}$	$0.97^{+0.03}_{-0.02}$	-0.18 ± 0.10	$4.308^{+0.007}_{-0.005}$	$0.36^{+0.04}_{-0.04}$	$58.2^{+21.0}_{-16.3}$	$27.2^{+5.7}_{-7.0}$	0	MS	L
9139151	6302 ± 77	$1.32^{+0.75}_{-0.94}$	$1.18^{+0.04}_{-0.03}$	0.10 ± 0.10	$4.382^{+0.008}_{-0.008}$	$0.95^{+0.04}_{-0.04}$	$73.5^{+11.0}_{-11.0}$	$11.6^{+0.8}_{-1.1}$	0	H	L
9139163	6400 ± 84	$1.60^{+0.22}_{-0.22}$	$1.40^{+0.03}_{-0.05}$	0.15 ± 0.09	$4.200^{+0.008}_{-0.009}$	$1.59^{+0.07}_{-0.08}$	$33.5^{+3.0}_{-3.0}$	$4.0^{+0.3}_{-0.3}$	1	H	L
9206432	6538 ± 77	$1.53^{+0.30}_{-0.21}$	$1.38^{+0.04}_{-0.04}$	0.16 ± 0.10	$4.220^{+0.005}_{-0.007}$	$1.55^{+0.17}_{-0.20}$	$34.3^{+5.7}_{-4.2}$	$4.1^{+1.0}_{-0.5}$	0	H	L
9353712	6278 ± 77	$2.15^{+0.11}_{-0.13}$	$1.51^{+0.03}_{-0.02}$	-0.05 ± 0.10	$3.943^{+0.007}_{-0.005}$	$0.75^{+0.16}_{-0.17}$	$37.6^{+29.1}_{-12.6}$	$9.5^{+7.3}_{-3.9}$	0	H	L
9410862	6047 ± 77	$6.93^{+1.49}_{-1.33}$	$0.97^{+0.05}_{-0.04}$	-0.31 ± 0.10	$4.300^{+0.009}_{-0.008}$	$0.41^{+0.09}_{-0.08}$	$46.4^{+28.3}_{-16.7}$	$20.6^{+9.8}_{-8.1}$	1	MS	L
9414417	6253 ± 75	$2.65^{+0.16}_{-0.18}$	$1.40^{+0.03}_{-0.03}$	-0.13 ± 0.10	$4.016^{+0.003}_{-0.005}$	$1.09^{+0.05}_{-0.05}$	$58.1^{+6.9}_{-9.7}$	$9.0^{+1.1}_{-0.9}$	0	H	L
9592705	6174 ± 92	$2.33^{+0.18}_{-0.16}$	$1.51^{+0.03}_{-0.02}$	0.22 ± 0.10	$3.961^{+0.004}_{-0.003}$	$0.93^{+0.09}_{-0.09}$	$59.3^{+17.8}_{-12.1}$	$10.7^{+2.1}_{-1.9}$	0	SG	K
9812850	6321 ± 77	$2.71^{+0.46}_{-0.35}$	$1.37^{+0.04}_{-0.05}$	-0.07 ± 0.10	$4.053^{+0.008}_{-0.009}$	$1.54^{+0.09}_{-0.08}$	$81.0^{+6.4}_{-10.0}$	$7.4^{+0.4}_{-0.5}$	0	H	L
9955598	5457 ± 77	$6.29^{+1.95}_{-1.84}$	$0.90^{+0.04}_{-0.03}$	0.05 ± 0.10	$4.497^{+0.007}_{-0.005}$	$0.29^{+0.04}_{-0.04}$	$53.4^{+20.8}_{-11.9}$	$31.4^{+9.1}_{-6.4}$	0	MS	L
9965715	5860 ± 180	$2.92^{+0.84}_{-0.75}$	$1.21^{+0.04}_{-0.05}$	-0.44 ± 0.18	$4.272^{+0.008}_{-0.009}$	$1.75^{+0.05}_{-0.05}$	$58.3^{+3.5}_{-3.2}$	$5.6^{+0.3}_{-0.3}$	0	MS	L
10068307	6132 ± 77	$2.36^{+0.10}_{-0.08}$	$1.47^{+0.02}_{-0.02}$	-0.23 ± 0.10	$3.967^{+0.004}_{-0.004}$	$0.71^{+0.03}_{-0.03}$	$41.7^{+6.0}_{-4.1}$	$10.9^{+1.5}_{-1.1}$	0	SG	L
10079226	5949 ± 77	$3.06^{+0.70}_{-0.65}$	$1.12^{+0.03}_{-0.02}$	0.11 ± 0.10	$4.366^{+0.005}_{-0.005}$	$0.65^{+0.07}_{-0.08}$	$75.1^{+10.6}_{-23.4}$	$16.8^{+2.2}_{-3.0}$	1	MS	L
10162436	6146 ± 77	$2.46^{+0.11}_{-0.10}$	$1.45^{+0.02}_{-0.01}$	-0.16 ± 0.10	$3.981^{+0.005}_{-0.005}$	$0.84^{+0.05}_{-0.05}$	$25.5^{+2.1}_{-1.8}$	$5.9^{+0.6}_{-0.6}$	0	SG	L
10454113	6177 ± 77	$2.89^{+0.56}_{-0.53}$	$1.17^{+0.02}_{-0.03}$	-0.07 ± 0.10	$4.314^{+0.005}_{-0.005}$	$0.76^{+0.07}_{-0.07}$	$40.9^{+26.9}_{-9.6}$	$10.0^{+4.8}_{-2.5}$	0	MS	L
10514430	5784 ± 98	$7.84^{+0.40}_{-0.91}$	$1.06^{+0.04}_{-0.04}$	-0.11 ± 0.11	$4.061^{+0.004}_{-0.004}$	$0.18^{+0.05}_{-0.05}$	$57.2^{+23.5}_{-32.0}$	$53.6^{+23.6}_{-27.2}$	1	MS	K
10516096	5964 ± 77	$7.01^{+1.33}_{-1.45}$	$1.06^{+0.05}_{-0.06}$	-0.11 ± 0.10	$4.169^{+0.010}_{-0.011}$	$0.48^{+0.03}_{-0.05}$	$71.8^{+12.5}_{-16.2}$	$22.6^{+1.9}_{-3.1}$	0	MS	L
10586004	5770 ± 83	$6.43^{+0.64}_{-0.61}$	$1.18^{+0.03}_{-0.03}$	0.29 ± 0.10	$4.071^{+0.005}_{-0.005}$	$0.48^{+0.16}_{-0.17}$	$59.3^{+20.6}_{-22.4}$	$19.6^{+11.1}_{-6.5}$	1	MS	K
10644253	6045 ± 77	$2.39^{+1.12}_{-0.96}$	$1.10^{+0.04}_{-0.04}$	0.06 ± 0.10	$4.396^{+0.007}_{-0.008}$	$0.24^{+0.08}_{-0.08}$	$55.6^{+24.0}_{-30.3}$	$38.0^{+21.1}_{-19.1}$	0	MS	L
10666592	6350 ± 80	$2.11^{+0.29}_{-0.24}$	$1.50^{+0.04}_{-0.04}$	0.26 ± 0.08	$4.017^{+0.008}_{-0.007}$	$0.91^{+0.11}_{-0.11}$	$47.2^{+27.2}_{-14.8}$	$9.5^{+3.6}_{-3.2}$	0	H	K
10730618	6150 ± 180	$3.05^{+0.46}_{-0.29}$	$1.34^{+0.05}_{-0.04}$	-0.11 ± 0.18	$4.062^{+0.008}_{-0.007}$	$0.56^{+0.23}_{-0.25}$	$55.6^{+23.7}_{-26.2}$	$16.1^{+13.9}_{-7.2}$	0	MS	L
10963065	6140 ± 77	$7.15^{+1.92}_{-1.61}$	$0.99^{+0.06}_{-0.06}$	-0.19 ± 0.10	$4.277^{+0.011}_{-0.011}$	$0.67^{+0.03}_{-0.03}$	$41.8^{+4.7}_{-3.6}$	$11.5^{+1.3}_{-1.0}$	0	MS	L
11081729	6548 ± 82	$1.88^{+0.59}_{-0.42}$	$1.30^{+0.05}_{-0.05}$	0.11 ± 0.10	$4.245^{+0.009}_{-0.010}$	$3.35^{+0.10}_{-0.10}$	$82.9^{+4.9}_{-5.9}$	$3.4^{+0.1}_{-0.1}$	0	H	L
11133306	5982 ± 82	$5.14^{+0.88}_{-0.86}$	$1.06^{+0.03}_{-0.03}$	-0.02 ± 0.10	$4.314^{+0.004}_{-0.007}$	$0.39^{+0.14}_{-0.13}$	$58.0^{+21.9}_{-24.1}$	$24.6^{+14.3}_{-10.0}$	0	MS	K
11253226	6642 ± 77	$1.60^{+0.06}_{-0.13}$	$1.41^{+0.02}_{-0.01}$	-0.08 ± 0.10	$4.173^{+0.005}_{-0.004}$	$2.55^{+0.11}_{-0.12}$	$49.3^{+6.3}_{-4.4}$	$3.4^{+0.4}_{-0.3}$	0	H	L
11295426	5793 ± 74	$6.31^{+0.32}_{-0.34}$	$1.07^{+0.01}_{-0.02}$	0.12 ± 0.07	$4.280^{+0.003}_{-0.003}$	$0.22^{+0.03}_{-0.03}$	$55.6^{+22.9}_{-20.9}$	$42.6^{+11.5}_{-14.5}$	0	MS	K
11401755	5911 ± 66	$7.10^{+0.61}_{-0.61}$	$1.06^{+0.03}_{-0.03}$	-0.20 ± 0.06	$4.039^{+0.005}_{-0.004}$	$0.55^{+0.09}_{-0.10}$	$64.6^{+17.4}_{-19.5}$	$18.5^{+4.7}_{-4.3}$	0	MS	K
11772920	5180 ± 180	$10.67^{+2.73}_{-2.97}$	$0.83^{+0.04}_{-0.04}$	-0.09 ± 0.18	$4.500^{+0.005}_{-0.008}$	$0.31^{+0.03}_{-0.04}$	$70.8^{+5.3}_{-14.3}$	$35.1^{+5.3}_{-4.7}$	1	MS	L

Table 1: *Continued from previous page.*

KIC	$T_{\rm eff}$ [K]	Age [Gyr]	Mass [M$_\odot$]	[Fe/H] [dex]	$\log(g)$ [dex]	$\nu_{\rm s}\sin(i)$ [μHz]	i [°]	P [days]	Flag	Type	Source
11807274	6225±75	$3.59^{+0.78}_{-0.45}$	$1.24^{+0.04}_{-0.04}$	0.00±0.08	$4.135^{+0.009}_{-0.007}$	$1.42^{+0.07}_{-0.07}$	$76.8^{+8.8}_{-9.4}$	$7.9^{+0.5}_{-0.5}$	0	MS	K
11853905	5781±76	$6.71^{+0.77}_{-0.67}$	$1.12^{+0.02}_{-0.03}$	0.09±0.10	$4.102^{+0.004}_{-0.005}$	$0.27^{+0.09}_{-0.09}$	$54.7^{+24.5}_{-28.8}$	$34.0^{+18.9}_{-17.2}$	1	MS	K
11904151	5647±74	$10.23^{+0.67}_{-0.83}$	$0.92^{+0.01}_{-0.02}$	-0.15±0.10	$4.344^{+0.003}_{-0.003}$	$0.24^{+0.06}_{-0.07}$	$64.9^{+18.1}_{-28.4}$	$40.9^{+16.5}_{-12.8}$	1	MS	K
12009504	6179±77	$3.97^{+0.57}_{-0.43}$	$1.17^{+0.02}_{-0.04}$	-0.08±0.10	$4.211^{+0.007}_{-0.005}$	$1.16^{+0.03}_{-0.04}$	$71.3^{+8.0}_{-5.7}$	$9.4^{+0.5}_{-0.5}$	0	MS	L
12069127	6276±77	$2.01^{+0.11}_{-0.13}$	$1.57^{+0.03}_{-0.02}$	0.08±0.10	$3.912^{+0.005}_{-0.004}$	$0.54^{+1.26}_{-0.33}$	$16.6^{+54.2}_{-6.3}$	$5.2^{+39.9}_{-3.9}$	1	H	L
12069424	5825±50	$6.67^{+0.81}_{-0.77}$	$1.05^{+0.02}_{-0.02}$	0.10±0.03	$4.287^{+0.007}_{-0.007}$	$0.40^{+0.01}_{-0.01}$	$44.7^{+6.2}_{-2.9}$	$20.5^{+2.0}_{-1.1}$	1	MS	L
12069449	5750±50	$7.39^{+0.89}_{-0.91}$	$0.99^{+0.02}_{-0.02}$	0.05±0.02	$4.353^{+0.005}_{-0.005}$	$0.31^{+0.01}_{-0.01}$	$34.0^{+3.0}_{-2.4}$	$21.2^{+1.8}_{-1.5}$	0	MS	L
12258514	5964±77	$4.05^{+0.18}_{-0.16}$	$1.26^{+0.01}_{-0.01}$	0.00±0.10	$4.126^{+0.008}_{-0.003}$	$0.39^{+0.04}_{-0.03}$	$35.0^{+22.9}_{-6.6}$	$16.7^{+10.0}_{-3.6}$	1	MS	L
12317678	6580±77	$2.46^{+0.22}_{-0.18}$	$1.34^{+0.04}_{-0.01}$	-0.28±0.10	$4.048^{+0.008}_{-0.009}$	$1.27^{+0.13}_{-0.14}$	$35.3^{+10.1}_{-5.2}$	$5.2^{+1.8}_{-0.9}$	0	H	L

References

[1] Davies, G. R. *et al.* Asteroseismic inference on rotation, gyrochronology and planetary system dynamics of 16 Cygni. *Mon. Not. R. Astron. Soc.* **446**, 2959–2966 (2015). `1411.1359`.

[2] Chaplin, W. J. *et al.* Ensemble Asteroseismology of Solar-Type Stars with the NASA Kepler Mission. *Science* **332**, 213 (2011). `1109.4723`.

[3] Harvey, J. High-Resolution Helioseismology. *Future Missions in Solar, Heliospheric & Space Plasma Physics* **235**, 199 (1985).

[4] Chaplin, W. J. & Basu. *Asteroseismic Data Analysis: Foundations and Techniques* (Princeton University Press, Princeton, New Jersey, 2017), 1st edn.

[5] Davies, G. R. *et al.* Oscillation frequencies for 35 Kepler solar-type planet-hosting stars using Bayesian techniques and machine learning. *Mon. Not. R. Astron. Soc.* **456**, 2183–2195 (2016). `1511.02105`.

[6] Lund, M. N. *et al.* Standing on the Shoulders of Dwarfs: The Kepler Asteroseismic LEGACY Sample. I. Oscillation Mode Parameters. *Astrophys. J.* **835**, 172 (2017).

[7] Tassoul, M. Asymptotic approximations for stellar nonradial pulsations. *Astrophys. J. Supplement Series* **43**, 469–490 (1980).

[8] Vrard, M., Mosser, B. & Samadi, R. Period spacings in red giants. II. Automated measurement. *Astron. Astrophys.* **588**, A87 (2016).

[9] Hogg, D. W. Data analysis recipes: Probability calculus for inference. *arXiv e-prints* arXiv:1205.4446 (2012).

[10] Hall, O. J. *et al.* Testing asteroseismology with Gaia DR2: Hierarchical models of the Red Clump. *Mon. Not. R. Astron. Soc.* **486**, 3569–3585 (2019). `1904.07919`.

[11] Mazumdar, A. *et al.* Measurement of acoustic glitches in solar-type stars from oscillation frequencies observed by Kepler. *Astrophys. J.* **782**, 18 (2014). `1312.4907`.

[12] Davies, G. R., Chaplin, W. J., Elsworth, Y. & Hale, S. J. BiSON data preparation: A correction for differential extinction and the weighted averaging of contemporaneous data. *Mon. Not. R. Astron. Soc.* **441**, 3009–3017 (2014).

[13] Appourchaux, T. *et al.* Oscillation mode linewidths and heights of 23 main-sequence stars observed by *Kepler (Corrigendum)*. *Astronomy & Astrophysics* **595**, C2 (2016).

[14] Rasmussen, C. E. & Williams, C. K. I. *Gaussian Processes for Machine Learning.* Adaptive Computation and Machine Learning (MIT Press, Cambridge, Mass, 2006).

[15] Toutain, T. & Appourchaux, T. Maximum likelihood estimators: An application to the estimation of the precision of helioseismic measurements. *Astron. Astrophys.* **289**, 649–658 (1994).

[16] Gizon, L. & Solanki, S. K. Determining the Inclination of the Rotation Axis of a Sun-like Star. *Astrophys. J.* **589**, 1009 (2003).

[17] Handberg, R. & Campante, T. L. Bayesian peak-bagging of solar-like oscillators using MCMC: A comprehensive guide. *Astron. Astrophys.* **527**, A56 (2011).

[18] Appourchaux, T., Gizon, L. & Rabello-Soares, M.-C. The art of fitting p-mode spectra. I. Maximum likelihood estimation. *Astron. Astrophys. Supplement Series* **132**, 107–119 (1998).

[19] Anderson, E. R., Duvall, J., Thomas L. & Jefferies, S. M. Modeling of Solar Oscillation Power Spectra. *Astrophys. J.* **364**, 699 (1990).

[20] Van Hoey, S., van der Kwast, J., Nopens, I. & Seuntjens, P. Python package for model STructure ANalysis (pySTAN). *EGU General Assembly Conference Abstracts* **15**, EGU2013–10059 (2013).

[21] Salvatier, J., Wiecki, T. V. & Fonnesbeck, C. Probabilistic programming in Python using PyMC3. *PeerJ Computer Science* **2**, e55 (2016).

[22] Gelman, A. Prior distributions for variance parameters in hierarchical models (comment on article by Browne and Draper). *Bayesian Analysis* **1**, 515–534 (2006).

[23] Ballot, J., Garcia, R. A. & Lambert, P. Rotation speed and stellar axis inclination from p modes: How CoRoT would see other suns. *Mon. Not. R. Astron. Soc.* **369**, 1281–1286 (2006).

[24] Ballot, J., Appourchaux, T., Toutain, T. & Guittet, M. On deriving p-mode parameters for inclined solar-like stars. *Astronomy & Astrophysics* **486**, 867–875 (2008). 0803.0885.

[25] Kass, R. E. & Raftery, A. E. Bayes Factors. *Journal of the American Statistical Association* **90**, 773–795 (1995).

[26] Nielsen, M. B., Schunker, H., Gizon, L. & Ball, W. H. Constraining differential rotation of Sun-like stars from asteroseismic and starspot rotation periods. *Astron. Astrophys.* **582**, A10 (2015).

[27] Benomar, O. *et al.* Asteroseismic detection of latitudinal differential rotation in 13 Sun-like stars. *Science* **361**, 1231–1234 (2018). 1809.07938.

[28] Beck, J. G. A comparison of differential rotation measurements - (Invited Review). *Solar Physics* **191**, 47–70 (2000).

[29] Benomar, O., Takata, M., Shibahashi, H., Ceillier, T. & García, R. A. Nearly uniform internal rotation of solar-like main-sequence stars revealed by space-based asteroseismology and spectroscopic measurements. *Mon. Not. R. Astron. Soc.* **452**, 2654–2674 (2015).

[30] Doyle, A. P., Davies, G. R., Smalley, B., Chaplin, W. J. & Elsworth, Y. Determining stellar macroturbulence using asteroseismic rotational velocities from Kepler. *Mon. Not. R. Astron. Soc.* **444**, 3592–3602 (2014).

[31] Tayar, J. *et al.* Rapid Rotation of Low-mass Red Giants Using APOKASC: A Measure of Interaction Rates on the Post-main-sequence. *Astrophys. J.* **807**, 82 (2015).

[32] Schofield, M. *et al.* The Asteroseismic Target List for Solar-like Oscillators Observed in 2 minute Cadence with the Transiting Exoplanet Survey Satellite. *Astrophys. J. Supplement Series* **241**, 12 (2019).

[33] Mathur, S. *et al.* Revisiting the impact of stellar magnetic activity on the detection of solar-like oscillations by Kepler. *Frontiers in Astronomy and Space Sciences* **6**, 46 (2019). 1907.01415.

[34] van Saders, J. L., Pinsonneault, M. H. & Barbieri, M. Forward Modeling of the Kepler Stellar Rotation Period Distribution: Interpreting Periods from Mixed and Biased Stellar Populations. *Astrophys. J.* **872**, 128 (2019).

[35] Amard, L. & Matt, S. P. The Impact of Metallicity on the Evolution of the Rotation and Magnetic Activity of Sun-like Stars. *Astrophys. J.* **889**, 108 (2020). 2001.10404.

[36] van Saders, J. L. & Pinsonneault, M. H. Fast Star, Slow Star; Old Star, Young Star: Subgiant Rotation as a Population and Stellar Physics Diagnostic. *Astrophys. J.* **776**, 67 (2013).

[37] Matt, S. P., Brun, A. S., Baraffe, I., Bouvier, J. & Chabrier, G. The Mass-dependence of Angular Momentum Evolution in Sun-like Stars. *Astrophys. J.* **799**, L23 (2015).

[38] Silva Aguirre, V. *et al.* Ages and fundamental properties of Kepler exoplanet host stars from asteroseismology. *Mon. Not. R. Astron. Soc.* **452**, 2127–2148 (2015). 1504.07992.

[39] Leiner, E., Mathieu, R. D., Vanderburg, A., Gosnell, N. M. & Smith, J. C. Blue Lurkers: Hidden Blue Stragglers on the M67 Main Sequence Identified from Their Kepler/K2 Rotation Periods. *Astrophys. J.* **881**, 47 (2019). 1904.02169.

[40] Fleming, D. P., Barnes, R., Davenport, J. R. A. & Luger, R. Rotation Period Evolution in Low-mass Binary Stars: The Impact of Tidal Torques and Magnetic Braking. *Astrophys. J.* **881**, 88 (2019).

[41] Halbwachs, J. L. Common proper motion stars in the AGK 3. *Astron. Astrophys.s* **66**, 131–148 (1986).

[42] White, T. R. *et al.* Interferometric radii of bright Kepler stars with the CHARA Array: θ Cygni and 16 Cygni A and B. *Mon. Not. R. Astron. Soc.* **433**, 1262–1270 (2013). 1305.1934.

[43] Maxted, P. F. L., Serenelli, A. M. & Southworth, J. Comparison of gyrochronological and isochronal age estimates for transiting exoplanet host stars. *Astron. Astrophys.* **577**, A90 (2015).

[44] Gallet, F. & Delorme, P. Star-planet tidal interaction and the limits of gyrochronology. *Astron. Astrophys.* **626**, A120 (2019). 1905.06070.

[45] Benbakoura, M., Réville, V., Brun, A. S., Le Poncin-Lafitte, C. & Mathis, S. Evolution of star-planet systems under magnetic braking and tidal interaction. *Astron. Astrophys.* **621**, A124 (2019).

[46] Ceillier, T. *et al.* Rotation periods and seismic ages of KOIs - comparison with stars without detected planets from Kepler observations. *Mon. Not. R. Astron. Soc.* **456**, 119–125 (2016).

[47] Silva Aguirre, V. *et al.* Standing on the Shoulders of Dwarfs: The Kepler Asteroseismic LEGACY Sample. II.Radii, Masses, and Ages. *Astrophys. J.* **835**, 173 (2017).